Available online at www.sciencedirect.com
ScienceDirect
Surface & Coatings Technology 201 (2006) 3701–3708
SURFACE & COATINGS TECHNOLOGY
www.elsevier.com/locate/surfcoat

# Investigation on the effect of benzotriazole on the phosphating of carbon steel

E.P. Banczek [a], P.R.P. Rodrigues [b], I. Costa [a,*]

[a] Instituto de Pesquisas Energéticas e Nucleares IPEN/CNEN-SP - Centro de Ciência e Tecnologia de Materiais – São Paulo, Brazil
[b] Universidade Estadual do Centro-Oeste, Departamento de Química/Unicentro-Guarapuava, Brazil

Received 25 July 2006; accepted in revised form 4 September 2006
Available online 23 October 2006

**Abstract**

Phosphating and corrosion inhibitors are commonly used for corrosion prevention of metallic materials, mainly carbon steels. In this study, the effect of benzotriazole (BTAH) added to a Zinc phosphating (PZn) bath on the corrosion resistance of a carbon steel (1010) was investigated. Anodic polarization curves and electrochemical impedance spectroscopy (EIS) were used to evaluate the corrosion resistance of the phosphated steel with or without BTAH, in two solutions, 0.1 mol $L^{-1}$ $H_2SO_4$ and 0.5 mol $L^{-1}$ NaCl. The results showed better corrosion resistance for the steel phosphated with BTAH comparatively to that without BTAH.


*Keywords:* Phosphating; Inhibitors; Benzotriazole; Corrosion; Carbon steel

## 1. Introduction

Phosphating is a conversion coating treatment largely used in many industries as a surface preparation for coating by paints and to increase corrosion resistance [1]. Phosphate layer on ferrous or non-ferrous metals [2–6] improve their surface properties by changes in the physico-chemical properties. The main applications of phosphating are for paints adhesion, to increase corrosion resistance, to oil impregnation and to promote electrical insulation [7,8].

Despite of their use for corrosion protection, phosphate layers by themselves do not produce considerable improvements in the metallic substrate corrosion resistance and need to be associated with other corrosion protection methods.

Phosphating processes have been developed for many years, using various additives, such as: nitrites, nitrates, chlorates, hydroxylamines, citric acids, calcium, nickel and manganese [9,10]. These additives are used as accelerators or to improve the properties of the phosphate layers.

The addition of organic compounds to phosphating baths has also been largely reported [9,10]. The researches show that these additives cause the improvement in corrosion resistance and decrease the porosity of the phosphate layer [11].

The effect of triazolic compounds as additives for phosphating baths on the corrosion resistance of the metallic substrate was investigated in this study. These compounds are widely used as corrosion inhibitors of various metals in different environments [12–14], mainly for copper and ferrous alloys; among them the most extensively used are benzotriazole BTAH [15–19] and tolytriazole (TTAH) [20]. However, the use of these compounds in phosphating baths has not yet been reported, with the exception of the work of Banczek et al. [21]. Those authors [21] investigated used TTAH as additive in phosphating baths for carbon steel and found that it caused the increase in the corrosion resistance of the phosphated steel comparatively to that phosphated in a bath without this additive.

The aim of this study was to evaluate the viability of using BTAH as additive in zinc phosphating baths for carbon steel, and to investigate the corrosion resistance of the phosphated substrate in two types of electrolytes, and acid and a neutral one.

## 2. Experimental

### 2.1. Samples preparation

Samples with 60 × 60 × 2 mm of carbon steel SAE 1010, composition shown in Table 1, were used as substrate for phosphating.

* Corresponding author. Av. Prof. Lineu Prestes, 2242, CEP 05508-900, São Paulo-SP-Brazil. Tel.: +55 11 3816 9356; fax: +55 11 3816 9370.
*E-mail address:* icosta@ipen.br (I. Costa).

0257-8972/$ - see front matter © 2006 Elsevier B.V. All rights reserved.
doi:10.1016/j.surfcoat.2006.09.003

Table 1
Chemical composition of steel (SAE 1010) used as substrate for phosphating

| Element | Composition (wt.%) |
|---|---|
| C | 0.118 |
| Si | 0.023 |
| Mn | 0.310 |
| P | 0.020 |
| S | 0.016 |
| Cr | 0.024 |
| Ni | 0.028 |
| Mo | 0.002 |

The surface of the samples was prepared for phosphating by grinding with SiC papers successively from #220, #320, #400 to #600. After grinding, the samples were degreased with commercial alkaline cleaning solution and then rinsed. Subsequently, the samples were immersed in an alkaline solution titanated with a commercial compound, that is, a titanium phosphate salt in the concentration of 3 g/L (pH = 7.5–9.0), for 90 s at (25 ± 2) °C for surface activation. Next, the samples were immersed in a zinc phosphate PZn bath for 5 min at 25 °C, and then dried and weighed, obtaining $m_1$. For determination of the phosphate deposited mass ($m_2$), the phosphate coating was solubilized in 0.5 g/L chromium trioxide solution. The mass of phosphate layer was estimated by the following equation:

$$m_{\text{phosphate}} = \frac{m_1 - m_2}{A} \quad (1)$$

where $m_1$ is the mass of the phosphated steel, $m_2$ is the mass after phosphate layer solubilization, and $A$ is the surface area exposed to the phosphating bath.

The chemical composition of the concentrated zinc phosphating bath used in this study is shown in Table 2.

### 2.2. Phosphate layer characterization

The morphology of the phosphate layer was investigated by scanning electron microscopy (SEM) using a Philips XL30 microscope. The electrochemical behaviour of the phosphated samples was analyzed by electrochemical impedance spectroscopy and polarization curves, using a frequency response analyzer (Gamry model EIS 300) coupled to a PCI4/300 potentiostat. Electrodes with 2 $cm^2$ of geometrical area were used in the electrochemical tests. The references electrodes used were Ag/AgCl in the sodium chloride solution, and $Hg/Hg_2SO_4$ in the acid solution. A Pt wire was used as the auxiliary electrode. Two electrolytes were used for electrochemical characterization, a 0.1 mol $L^{-1}$ $H_2SO_4$ (pH = 0.4) and a 0.5 mol $L^{-1}$ NaCl solution (pH = 6.0), both at (20 ± 2) °C. The aim of using these two test solutions was to evaluate the resistance of the phosphate layer in highly aggressive acid media and in nearly neutral and aerated solutions. All reagents used were analytical grade and bidistilled water was used in the electrolytes preparation.

The electrochemical impedance spectroscopy (EIS) tests were carried out potentiostatically at $E_{corr}$, with voltage perturbation amplitude of 10 mV in the frequency range from 100 kHz to 10 mHz, with an acquisition rate of 10 points per decade.

The potentiodynamic polarization curves were obtained from $E_{corr}$ until −650 mV with a scan rate of 1 mV.$s^{-1}$ in both electrolytes.

Table 2
Chemical composition of the concentrated phosphating bath used

| Composition of zinc phosphating bath | (wt.%) |
|---|---|
| $H_3PO_4$ | 33 |
| $HNO_3$ | 23 |
| ZnO | 16 |
| $NiCO_3$ | 0.5 |
| $H_2O_2$ | 0.1 |
| $H_2O$ | 27.4 |

## 3. Results and discussion

### 3.1. Mass of deposited phosphate layer

The average mass of phosphate layer obtained after surface activation during 90 s, in the two phosphating baths, either with (PZn + BTAH) or without PZn additive, and estimated by gravimetric measurements is shown in Table 3.

The mass of phosphate obtained in PZn + BTAH indicates that a thicker layer was formed in this bath comparatively to that in the PZn one.

### 3.2. Morphological evaluation of phosphate layers.

Fig. 1 shows the morphologies of the steel substrate surface (a) and of the phosphate layer obtained in the two solutions, (b) in PZn and (c) in PZn + BTAH. The energy dispersive spectroscopy (EDS) spectra of the phosphate layers are also presented. This figure shows that the phosphate grains are deposited as hexagonal plates and present a needle-like morphology.

The semi-quantitative elemental composition obtained from the EDS analysis on the phosphate layers are shown in Table 4. The results show that the presence of BTAH in the phosphating bath did not affect the phosphate layer composition.

The mean size of the needle-shaped crystals estimated using SEM and measuring various crystals in the phosphate layers obtained either in PZn or PZn + BTAH phosphating baths, were (7 ± 3) μm and (4.5 ± 2) μm, respectively. These results suggest that the BTAH causes the decrease in the phosphate crystal size. The EDS spectra show that the phosphate layers contain mainly iron, zinc and phosphorus. The high peak of iron is mainly due to the metallic substrate.

Table 3
Average mass of phosphate layer obtained in PZn or PZn + BTAH phosphating solutions

| Phosphate layer obtained in | Average mass ($g/m^2$) |
|---|---|
| PZn | 2.13 ± 0.28 |
| PZn + BTAH | 2.48 ± 0.17 |

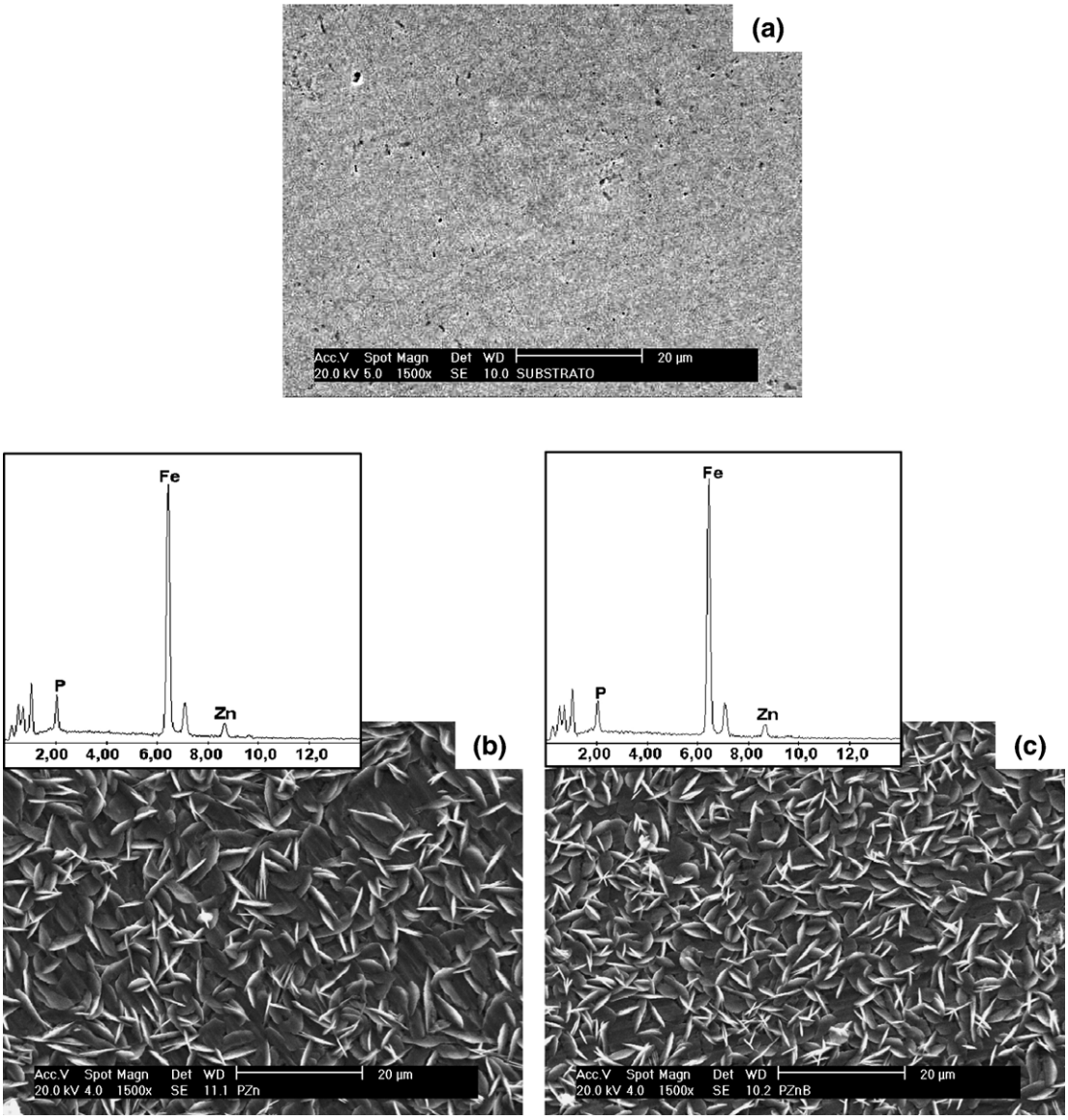


Fig. 1. Scanning electron micrographies of (a) SAE 1010 carbon steel, and phosphate layer obtained (b) in PZn, (c) in PZn+BTAH and corresponding EDS spectra.

The lower crystal sizes obtained in the solution with BTAH indicate that this additive has an effect on surface activation, favouring phosphate nucleation and leading to smaller crystals.

### 3.3. Electrochemical characterization

#### 3.3.1. In acid solution

The anodic polarization curves of the SAE 1010 carbon steel, either unphosphated or phosphated obtained in 0.1 mol $L^{-1}$ $H_2SO_4$ solution are shown in Fig. 2. The current densities for the phosphated samples are slightly lower than for the carbon steel substrate. However, all samples presented high current densities,

Table 4
Semi-quantitative elemental composition of zinc phosphate layers obtained in solutions with or without BTAH addition

| Element (wt.%) | Layer | |
|---|---|---|
| | PZn | PZn+BTAH |
| P | 5.09±0.31 | 4.77±0.12 |
| Fe | 83.48±0.67 | 83.85±0.44 |
| Zn | 11.43±1.03 | 11.39±0,32 |

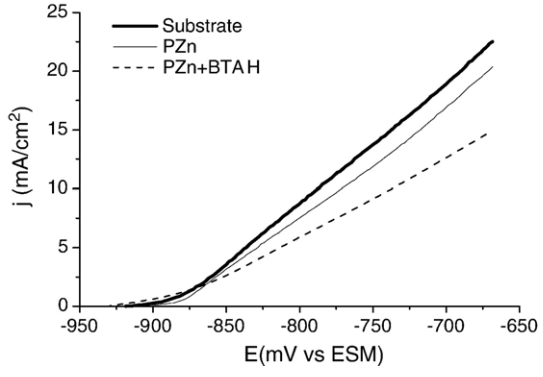


Fig. 2. Potentiodynamic anodic polarization curves in 0.1 mol $L^{-1}$ $H_2SO_4$ of SAE 1010 carbon steel, phosphated or unphosphated.

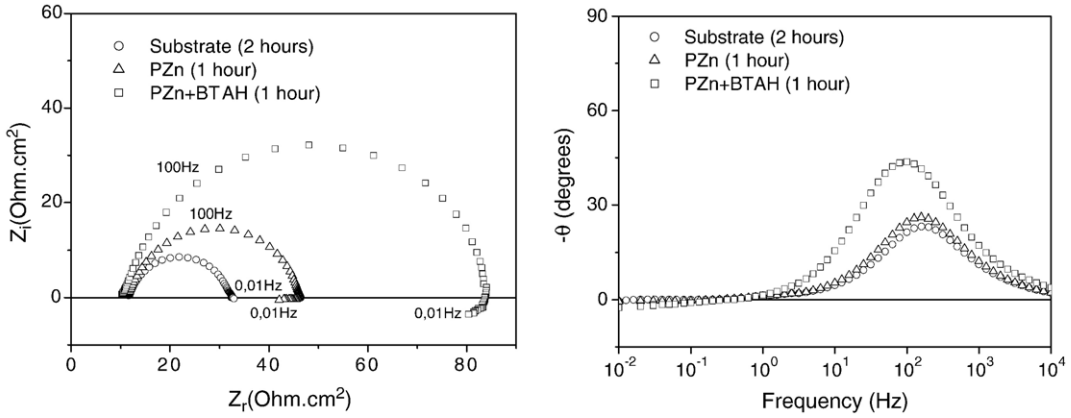


Fig. 3. Nyquist and Bode phase angle diagrams obtained after 1 h immersion in 0.1 mol $L^{-1}$ $H_2SO_4$ solution for the carbon steel, either unphosphated or phosphated in the baths with or without BTAH.

typical of active dissolution, showing that the phosphate layer did not cause surface passivation in the acid medium.

The results clearly indicated that the phosphate layer is easily attacked in the acid solution, and this indication was confirmed by surface observation after polarization tests. This is a shortcoming of this layer for the corrosion protection of the metallic substrate [22], leading to its direct exposure to the corrosive environment.

The EIS results for the phosphated or unphosphated samples in 0.1 mol.$L^{-1}$ $H_2SO_4$ solution are shown in Fig. 3 as Nyquist and Bode phase angle diagrams. The Nyquist diagrams indicate a capacitive semicircle suggesting only one time constant, and this is also supported by the Bode diagrams that show only a phase angle peak at frequencies around 100 Hz. The data obtained for the phosphated samples at low frequencies indicated an inductive behavior for all samples in the acid electrolyte. This has been related in literature to iron dissolution [23], due to the substrate attack since the first hours of immersion of the phosphated steel, also supporting the low resistance of the phosphate layer in the acid electrolyte.

The influence of immersion time in 0.1 mol $L^{-1}$ $H_2SO_4$ solution for the phosphated or unphosphated samples is shown in Fig. 4 as Nyquist and Bode phase angle diagrams.

The phosphated sample shows initially higher impedances than the substrate in the acid electrolyte, however after 2 h of immersion most of the phosphate layer was removed from the substrate, and after 3 h it was practically totally eliminated and similar impedance values were obtained for the phosphated and unphosphated steel. The results (not shown) indicated that for the sample phosphated in PZn, the phosphate layer was detached from the surface after only 2 h of immersion in the acid electrolyte. The slightly longer period for phosphate layer removal from the sample phosphated in PZn+BTAH was expected once the results in Table 3 showed higher mass associated to this sample comparatively to that phosphated in PZn.

The solubilization of the phosphate layer in the acid medium was confirmed by surface observation and EDS spectra after 2 h of immersion in this electrolyte, as shown in Fig. 5, for previously phosphated samples. The samples surface and EDS results after polarization in 0.1 mol $L^{-1}$ $H_2SO_4$ solution are also shown in this figure.

The EDS spectra presented in Fig. 5 show only the peak corresponding to Fe indicating the total removal of the phosphate layer.

The high aggressiveness of this medium to the phosphate layer shows that it is not appropriate for use under such

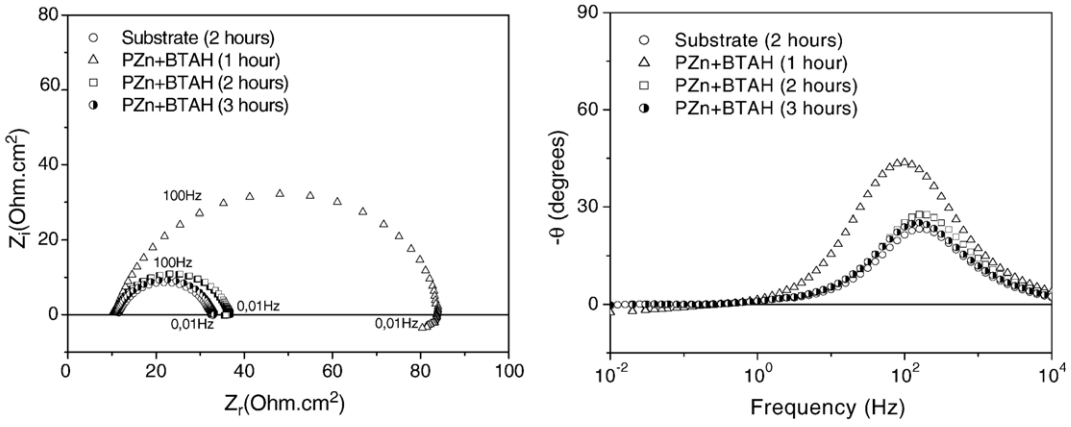


Fig. 4. Nyquist and Bode phase angle diagrams for carbon steel, unphosphated or phosphated in BTAH containing solution and effect of time of immersion in 0.1 mol $L^{-1}$ $H_2SO_4$ on the phosphated sample.

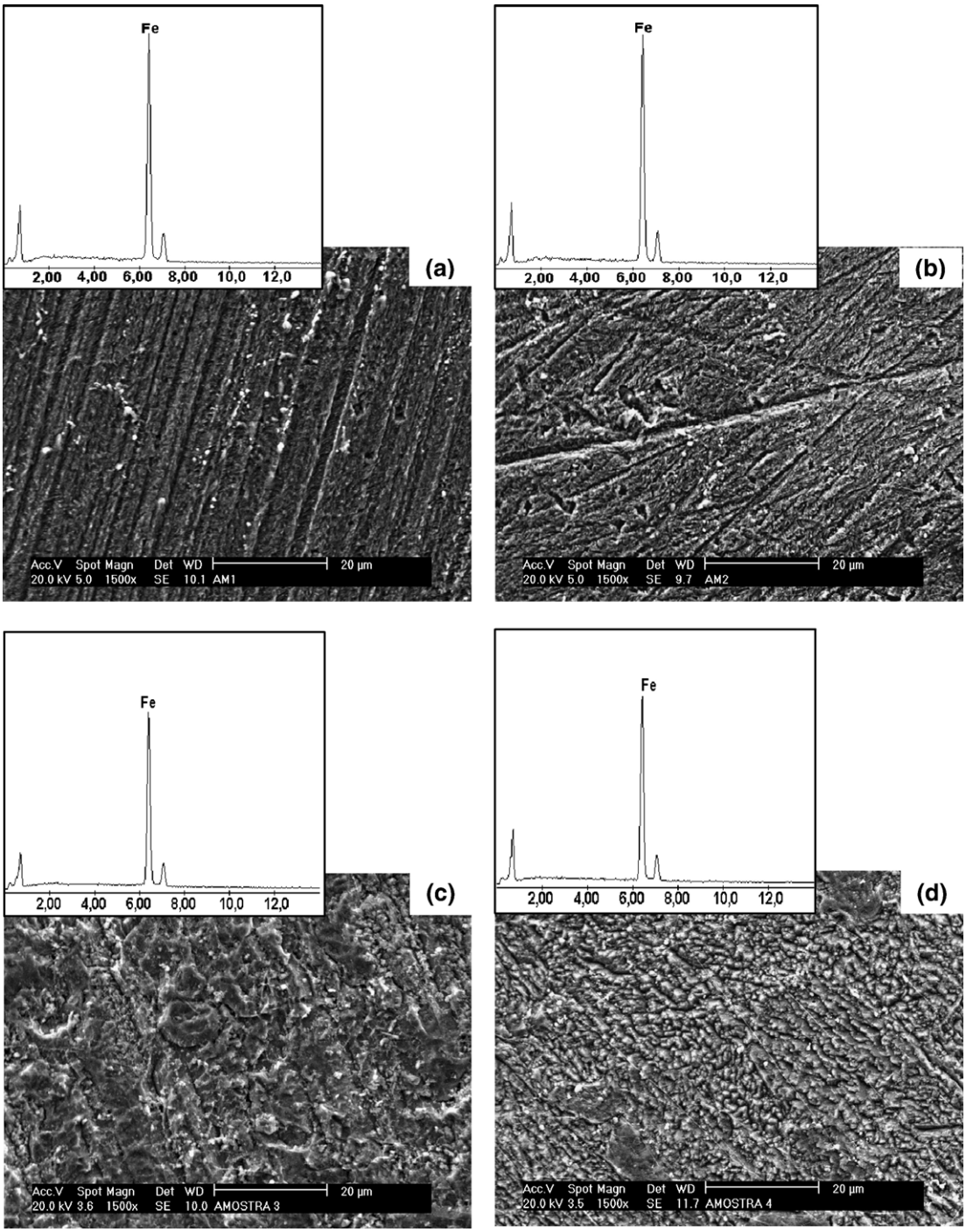


Fig. 5. Micrographies and EDS spectra of the phosphated samples after 2 h of immersion in 0.1 mol $L^{-1}$ $H_2SO_4$ solution. Sample previously phosphated (a) in PZn, (b) in PZn+BTAH, (c) in PZn after polarization (d) in PZn+BTAH after polarization.

conditions. The behavior of this layer in a neutral medium containing chloride was then evaluated.

### 3.3.2. In neutral solution

Cathodic polarization curves were obtained in 0.5 mol $L^{-1}$ NaCl solution and the results are shown in Fig. 6. A limiting current density ($i_L$) was obtained for all the samples, phosphated or unphosphated, in this medium, showing a diffusion controlled cathodic process, and the $i_L$ values decreased for the phosphated layers, the smallest values associated to the phosphate layer obtained in PZn+BTAH. This result suggests that the BTAH causes the polarization of the cathodic oxygen reduction reaction.

Corrosion rates ($i_{corr}$) were estimated by extrapolation of the linear segment of the cathodic curve to the corrosion potential. The average corrosion potential ($E_{corr}$) and ($i_{corr}$) values estimated from three measurements and also the corrosion inhibition efficiencies ($\theta$) due to the phosphate layer are shown

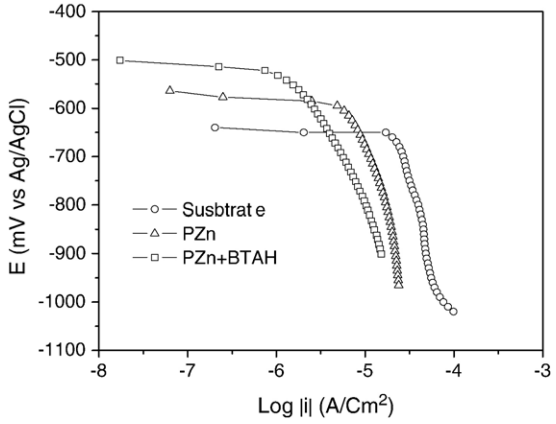


Fig. 6. Cathodic polarization curves obtained in 0.5 mol $L^{-1}$ NaCl solution for unphosphated and phosphated carbon steel.

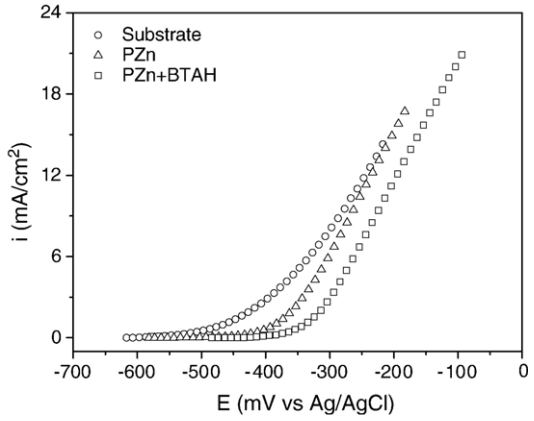


Fig. 7. Potentiodynamic anodic polarization curves obtained in 0.5 mol $L^{-1}$ NaCl solution for the carbon steel (SAE 1010) unphosphated or phosphate in PZn or PZn+BTAH.

in Table 5. The results presented in this table show that the phosphate layer moves the $E_{corr}$ into nobler values, suggesting that besides affecting the cathodic reaction it also influences the anodic reaction. It also shows that the efficiency associated to the phosphate layer formed in BTAH containing solution is significantly superior to that of the layer formed in the other solution.

Fig. 7 shows the potentiodynamic anodic polarization curves obtained in 0.5 mol $L^{-1}$ NaCl solution. A typical passive behavior is indicated for the phosphated samples at potentials close to $E_{corr}$, but the breakdown of this layer occurs at potentials of approximately −450 mV and −400 mV, for the phosphated samples obtained in PZn and PZn+BTAH, respectively.

Nyquist and Bode phase angle diagrams for the various tested samples in 0.5 mol $L^{-1}$ NaCl electrolyte are shown in Fig. 8. The Nyquist diagrams show for the phosphated samples two flattened capacitive semicircles and the Bode diagrams for the same samples show a large phase angle peak from high frequencies until approximately 10 Hz, suggesting the interaction of more than one time constant and at low frequencies another small peak. For the unphosphated substrate only a time constant is indicated by a peak at frequencies around 1 Hz.

The large peak at high frequencies and at phase angles lower than 60° is associated to the porous phosphate layer on the metallic substrate. The literature [24–27] reports that for porous electrodes, the high frequency response depends on the AC signal penetrability into the pores. When the AC signal does not penetrate as deep as the pores length, the signal detects only the pores and phase angles between 45° and 90° are obtained, depending on the pore's length. Large peaks at high frequencies with phase angles in the range from 50° to 60° were associated to porous corrosion products deposited on Nd–Fe–B magnets immersed in sodium chloride solution [27]. The interaction of various time constants results in the much flattened semicircle obtained. The time constant at low frequencies is likely due to the corrosive attack of the exposed substrate. The Nyquist diagrams clearly show the beneficial effect of the phosphate

Table 5
Average values of $i_{corr}$, $E_{corr}$ and efficiency ($\theta$) obtained from polarization curves

| Sample | $i_{corr}$(μA/cm$^2$) | $E_{corr}$ (V) | $\theta$ (%) |
|---|---|---|---|
| Substrate | 28.3±3.25 | −0.597±0.02 | – |
| PZn | 5.33±1.32 | −0.555±0.09 | 81±2.2 |
| PZn+BTAH | 1.98±0.29 | −0.522±0.02 | 93±2.5 |

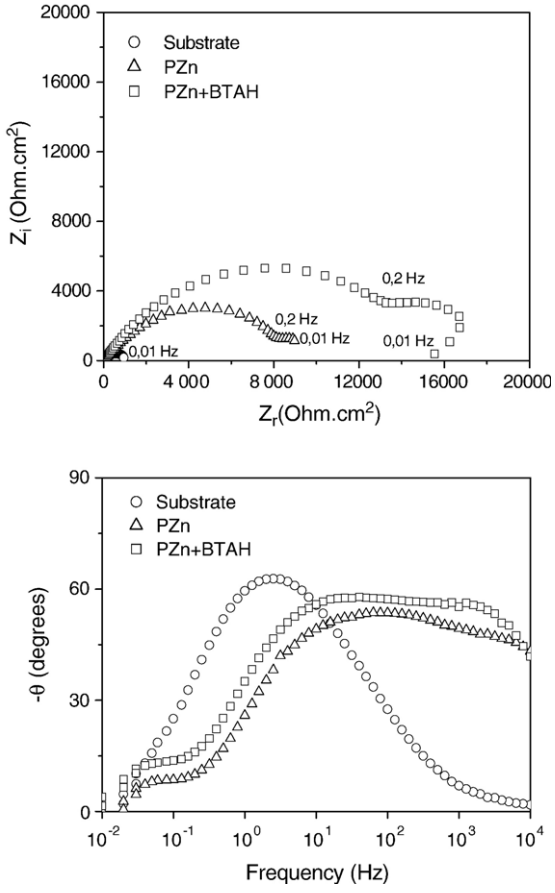


Fig. 8. Nyquist and Bode phase angle diagrams obtained after 2 h of immersion in 0.5 mol $L^{-1}$ NaCl solution, for unphosphated or phosphated carbon steel in PZn or PZn+BTAH.

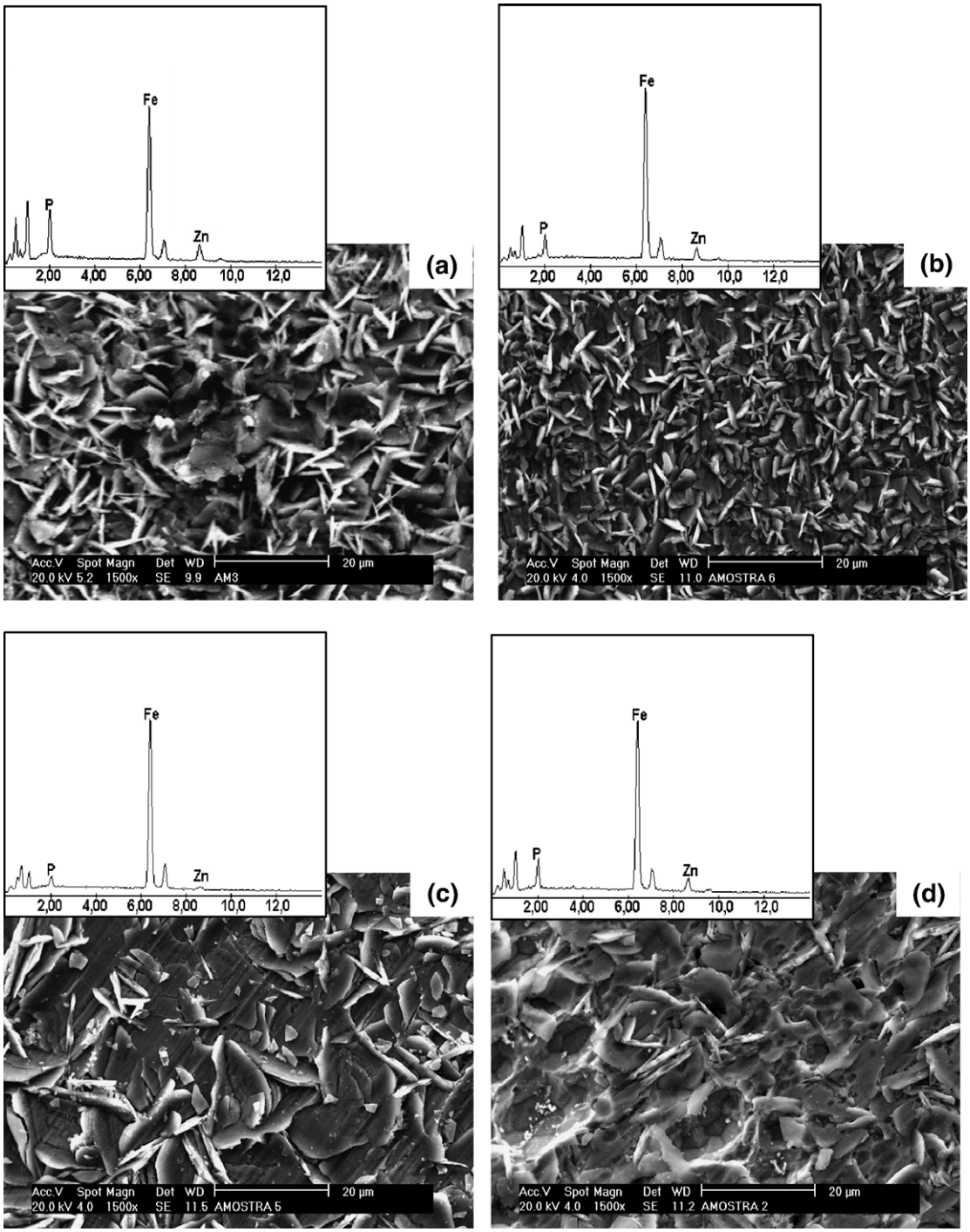


Fig. 9. Micrographies and EDS spectra of phosphated samples after 2 h of immersion in 0.5 mol $L^{-1}$ NaCl solution. Phosphate obtained in (a) (PZn) and (b) (PZn+BTAH) previous to polarization, and obtained in (c) (PZn) and (d) (PZn+BTAH) after polarization.

layer on the corrosion resistance of the 1010 carbon steel, causing a large increase in the impedance of the substrate, mainly that obtained in PZn+BTAH phosphating bath, supporting the previous presented results.

The surface of the various tested samples was observed by SEM and analysed EDS for a immersion period of 2 h in 0.5 mol $L^{-1}$ NaCl solution and the corresponding micrographies and EDS spectra are shown in Fig. 9.

In the sodium chloride medium after 2 h of immersion only localized attack was observed on the phosphated samples, mainly on the layer formed in PZn comparatively to that in PZn+BTAH.

The surface of the phosphated samples was also observed by SEM and analysed by EDS after polarization tests (Fig. 9 (c) and (d)) and the results showed that only partial removal of the phosphate layer occurred during polarization, and that the layer

formed in PZn+BTAH was more resistant to the corrosive attack.

The results indicate that the resistance of the phosphate layer to corrosive attack in the neutral chloride medium causes a large increase in the substrate corrosion resistance and that the incorporation of BTAH into the phosphating bath has a high beneficial effect to the corrosion properties of the obtained layer.

## 4. Conclusions

The phosphate layers obtained in this study showed very low corrosion resistance in the acid medium used (0.1 mol $L^{-1}$ $H_2SO_4$). In the sodium chloride neutral medium (0.5 mol $L^{-1}$ NaCl), however, the phosphate layers obtained in the PZn and PZn+BTAH solutions, showed high corrosion resistance, and the layer obtained in PZn+BTAH was significantly more resistant than that in PZn. The BTAH additive apparently favors phosphate nucleation resulting in particles of lower size and also in a more compact layer of higher weight than that formed in PZn, increasing the corrosion resistance of the metallic substrate.

## Acknowledgements

The authors are grateful to CNPq (Conselho Nacional de Desenvolvimento Científico e Tecnológico) for the grant provided to E.P. Banczek.

## References

[1] S. Rebeyrat, J.L.G. Poussard, J.F. Silvain, B. Panicaud, J.F. Dinhut, Appl. Surf. Sci. 199 (2002) 11.
[2] G. Lorin, Phosphating of Metals, Finishing Publications, Middlesex, 1974.
[3] Vicente Gentil, Corrosion, LTC, 3 th edition, Rio de Janeiro, 1987, pp. 319–384 (In Portuguese).
[4] S. Jegannathana, T.S.N. Sankara Narayanan, K. Ravichandrana, S. Rajeswaric, Surf. Coat. Technol. 200 (2006) 4117.
[5] M.F. Morks, Mater. Lett. 58 (2004) 3316.
[6] Yasar Totik, Surf. Coat. Technol. 200 (2004) 1.
[7] S. Palraj, M. Selvaraj, P. Jayakrishnan, Prog. Org. Coat. 54 (2005) 5.
[8] V. Burokas, A. Martusiene, G. Bikulcius, Surf. Coat. Technol. 102 (1998) 233.
[9] Guangyu Li, Liyuan Niu, Jianshe Lian, Zhonghao Jiang, Surf. Coat. Technol. 176 (2004) 215.
[10] Deliang He, Fancai Chen, Anhong Zhou, Lihuas Nie, Shouzhuo Yao, Thin Solid Films 382 (2001) 262.
[11] Madiha Shoeib, Magdi Farouk, Farid Hanna, Met. Finish. (1997) 62.
[12] F. Bentiss, M. Traisnel, L. Gengembre, M. Lagrenée, Appl. Surf. Sci. 161 (2000) 194.
[13] A. Guenbour, A. Kacemi, A. Benbachir, Prog. Org. Coat. 39 (2000) 151.
[14] D. Chebabe, Z. Ait Chikh, N. Haijjaji, A. Srhiri, F. Zucchi, Corros. Sci. 45 (2003) 309.
[15] A. Frignani, L. Tommesani, G. Brunoro, C. Monticelli, M. Fogagnolo, Corros. Sci., Part I 41 (1999) 1205.
[16] A. Frignani, M. Fonsati, C. Monticelli, G. Brunoro, Corros. Sci., Part I 41 (1999) 1217.
[17] Gamal K. Gomma, Mater. Chem. Phys. 55 (1998) 235.
[18] R.F.V. Vilamil, P. Corio, J.C. Rubim, S.M.L. Agostinho, J. Electroanal. Chem. 472 (1999) 112.
[19] S. Tamil Selvi, V. Raman, N. Rajendran, J. Appl. Electrochem. 33 (2003) 1175.
[20] S. Tamilselvi, S. Rajeswari, Anti-Corros. Methods Mat. 3 (2003) 223.
[21] E.P. Banczek, M.F. Oliveira, M.T. Cunha, P.R.P. Rodrigues, Port. Electrochim. Acta 23 (2005) 379.
[22] D. Weng, P. Jokiel, A. Uebleis, H. Boehni, Surf. Coat. Technol. 88 (1996) 147.
[23] I. Epelboin, O.R. Mattos, M. Keddam, H. Takenouti, Corros. Sci. 19 (1979) 1105.
[24] H.-K. Song, Y.-H. Jung, K.-H. Lee, L.H. Dao, Eletrochim. Acta 44 (1999) 3513.
[25] H.-K. Song, Y.-H. Yong, K.-H. Lee, L.H. Dao, Eletrochim. Acta 45 (2000) 2241.
[26] I.V. Aoki, M.C. Benard, S.I. Cordoba de Torresi, C. Deslouis, H.G. de Melo, S. Joiret, B. Tribollet, Eletrochim. Acta 46 (2001) 1871.
[27] I. Costa, M.C.L. Oliveira, H.G. Melo, R.N. Faria, J. Magn. Magn. Mater. 278 (2004) 348.